Determination of lower and upper bounds of predicted production from history-matched models

G.M. van Essen[2], S. Kahrobaei[1], H. van Oeveren[1], P.M.J. Van den Hof[3], J.D. Jansen[1]

[1] Delft University of Technology, The Netherlands
[2] Shell Global Solutions International B.V., Rijswijk, The Netherlands
[3] Eindhoven University of Technology, The Netherlands

Correspondence: j.d.jansen@tudelft.nl

Published in 2016 in *Computational Geosciences* **20** (5) 1061-1073. DOI: 10.1007/s10596-016-9576-1

http://link.springer.com/article/10.1007/s10596-016-9576-1

Abstract

We present a method to determine lower and upper bounds to the predicted production or any other economic objective from history-matched reservoir models. The method consists of two steps: 1) Performing a traditional computer-assisted history match of a reservoir model with the objective to minimize the mismatch between predicted and observed production data through adjusting the grid block permeability values of the model. 2) Performing two optimization exercises to minimize and maximize an economic objective over the remaining field life, for a fixed production strategy, by manipulating the same grid block permeabilities, however without significantly changing the mismatch obtained under step 1. This is accomplished through a hierarchical optimization procedure that limits the solution space of a secondary optimization problem to the (approximate) null-space of the primary optimization problem. We applied this procedure to two different reservoir models. We performed a history match based on synthetic data, starting from a uniform prior, and using a gradient-based minimization procedure. After history matching, minimization and maximization of net present value (NPV), using a fixed control strategy, were executed as secondary optimization problems by changing the model parameters while staying close to the null space of the primary optimization problem. In the other words we optimized the secondary objective functions, while requiring that optimality of the primary objective (a good history match) was preserved. This method therefore provides a way to quantify the economic consequences of the well-known problem that history matching is a strongly ill-posed problem. We also investigated how this method can be used as a means to assess the cost effectiveness of acquiring different data types to reduce the uncertainty in the expected NPV.

Key words

Computer-assisted history matching, uncertainty, hierarchical optimization, multi-objective optimization

1. Introduction

It is well-known that assimilation of production data into reservoir models is an ill-posed problem; see e.g. Watson et al.(1984), Tavassoli et al. (2004) or Oliver et al. (2008). This is mainly because generally the number of uncertain model parameters largely supersedes the number of measurements. Moreover, the measurements are strongly correlated because they originate from a relatively small number of sources: the wells. As a result, they contain less information about the true value of the model parameters than could be expected based solely on the number of data points. A relevant question in view of the purpose of large-scale, physics-based reservoir models is how much the long-term predictions can vary because of the ill-posedness of the assimilation problem. In other words, what may be the economic consequences of the lack of information about the reservoir in the measurements?

In most practical circumstances, this question is addressed by constructing and history-matching low and high case models, besides the nominal model. Alternatively, a set of model realizations can be used in a data-assimilation algorithm to obtain an entire collection of predictions, as is the case with ensemble Kalman filter (EnKF) methods, see, e.g., Evensen (2009) and Aanonsen et al. (2009). However, in either way the resulting history-matched models are heavily influenced by the prior information that went into the data-assimilation process. Hence, properly answering the question stated above requires either some (heuristic) method to translate static geological properties to flow behavior or economic performance, or requires many forward simulation runs to obtain a proper low or high case prior model. These methods may be either unreliable or impractical to provide a good measure of the economic consequences of the lack of knowledge about the true field.

In this paper a method is introduced to search for lower and upper bounds on predicted production (or any other economic objective) over the remaining life of a field, using a history-matched model.. The method consists of two steps: 1) Performing a traditional computer-assisted history match of a reservoir model with the objective to

minimize the mismatch between predicted and observed production data through adjusting the permeability values of the model. 2) Performing two optimization exercises to minimize and maximize an economic objective over the remaining field life, for a fixed production strategy, by manipulating the same grid block permeabilities, however without significantly changing the mismatch obtained under step 1. To achieve this we make use of the fact that history matching through adjusting grid block parameters is an ill-posed problem such that many combinations of parameter values may result in (nearly) identical mismatch values.

2. Problem definition

The problem of determining a history-matched model that provides either a lower or an upper bound on the predicted economic performance over the life of a reservoir is essentially a multi-objective optimization problem. For a general overview of multi-objective optimization, see, e.g., Marler and Arora (2004). The first objective is to find a certain realization of model parameters that minimizes the error between the measured and simulated production data, which can be expressed through a quantitative objective function V, e.g. mean square difference. The second objective relates to finding a set of parameter values that – for a certain future production strategy – minimizes or maximizes some economic cost function J, e.g. net present value (NPV). However, the multiple objectives are not of the same importance; priority lies with obtaining a good history-match, while determining a lower or upper bound on predicted economic performance serves as secondary objective. To that end, the multi-objective optimization problem may be cast into a hierarchical optimization problem, as presented in Haimes and Li (1988) and more recently specifically for oil production optimization in van Essen et al. (2011), Chen et al. (2012) and Fonseca et al. (2014). In this structure, optimization of a (secondary) economic cost function J is constrained by the requirement that the (primary) quantitative history-matching cost function V must remain close to its minimal value V_{min}. This requires solving the following two (hierarchical) optimization problems,

$$V_{\min} = \min_{\boldsymbol{\theta}} V\left(\boldsymbol{\theta}, \overline{\mathbf{u}}\right), \tag{1}$$

$$s.t. \quad \mathbf{g}_{k+1}\left(\overline{\mathbf{u}}_k, \mathbf{x}_k, \mathbf{x}_{k+1}, \boldsymbol{\theta}\right) = \mathbf{0}, \;\; k = 0, \ldots, K-1, \;\; \mathbf{x}_0 = \overline{\mathbf{x}}_0, \tag{2}$$

$$\mathbf{c}_{k+1}\left(\overline{\mathbf{u}}_{k+1}, \mathbf{x}_{k+1}, \boldsymbol{\theta}\right) \le \mathbf{0}, \tag{3}$$

and

$$\max_{\boldsymbol{\theta}} J\left(\boldsymbol{\theta}, \overline{\mathbf{u}}\right) \quad \text{or} \quad \min_{\boldsymbol{\theta}} J\left(\boldsymbol{\theta}, \overline{\mathbf{u}}\right), \tag{4}$$

$$s.t. \quad \mathbf{g}_{k+1}\left(\overline{\mathbf{u}}_k, \mathbf{x}_k, \mathbf{x}_{k+1}, \boldsymbol{\theta}\right) = \mathbf{0}, \;\; k = 0, \ldots, K-1, \;\; \mathbf{x}_0 = \overline{\mathbf{x}}_0, \tag{5}$$

$$\mathbf{c}_{k+1}\left(\overline{\mathbf{u}}_{k+1}, \mathbf{x}_{k+1}, \boldsymbol{\theta}\right) \le \mathbf{0}, \tag{6}$$

$$V\left(\boldsymbol{\theta}\right) - V_{min} \le \varepsilon, \tag{7}$$

where $\overline{\mathbf{u}}$ is the fixed control vector (input vector), $\mathbf{x}$ is the state vector (typically grid block pressures and saturations), $\mathbf{g}$ is a vector-valued function that represents the system equations, $\mathbf{x}_0$ is a vector of the initial conditions of the reservoir, the subscript k indicates discrete time, and K is the total number of time steps. The vector of inequality constraints $\mathbf{c}$ relates to the capacity limitations of the wells. The term ε is an arbitrary small value compared to V_{min}. In order to solve the secondary optimization problem, given in Eq. 4 to Eq. 7, first a (single) optimal solution to the primary optimization problem Eq. 1 to Eq. 3 is required to determine V_{min}. The optimal solution to the primary problem $\boldsymbol{\theta}_1^*$ can serve as feasible initial guess for the secondary problem. Note that the second optimization problem is also solved in terms of $\boldsymbol{\theta}$, while the values of the control $\overline{\mathbf{u}}$ remain unchanged. The search space of the secondary problem is now constrained by the null-space of the primary objective function at a value of V_{min}, through inequality constraint Eq. 7. In other words, the redundant degrees of freedom (DOF) of the primary problem are the DOF of the secondary problem. The motivation for using the constraint Eq. 7 is actually twofold. If ε is arbitrarily small (or even equal to 0) the parameter space that remains is actually the null space within the parameter space, which can be substantial because of the generally ill-posed nature of the inverse history-matching problem. Any changes of the model parameters within that null-space will have no effect on the value of the used quantitative history-match quality indicator, i.e. the objective function V. For $\varepsilon > 0$ the corresponding parameter space that satisfies Eq. 7 can be given the interpretation of a parameter uncertainty set, with a clear statistical interpretation, in the case of Gaussian noise disturbances on the data. The statistical uncertainty set then results from a hypothesis test based on the so-called likelihood ratio test, and is characterized by level sets of the likelihood function $V(\boldsymbol{\theta})$. See e.g. Quinn et al (2005) for the case of nonlinear models, and den Dekker et al. (2008) for linear models. This implies that under appropriate noise conditions, we

can, for every value of $\varepsilon > 0$, connect a probability level to the parameter uncertainty set defined by Eq. 7, and thus account for the variability of the history-matched parameters in the subsequent secondary economic optimization problem.

3. Methodology

In van Essen et al. (2011), the primary optimization problem is attacked using a gradient-based search algorithm. (Note that in that study the optimization variables were the inputs u, while here they are the model parameters $\boldsymbol{\theta}$.) The gradients are obtained using a system of adjoint equations which is solved backwards in time once, regardless of the number of optimization parameters. (See Jansen (2011) for an overview of adjoint-based optimization in porous media flow, and Kraaijevanger et al. (2007) for the specific implementation used in this study.) . Subsequently, the secondary optimization problem was also attacked using a gradient-based search algorithm. However, the secondary problem was executed with the addition of projecting the search direction onto a second-order approximation of the null-space with respect to the optimality constraint defined in equation (7). The second-order approximation was explicitly determined through a forward difference scheme using first-order information obtained with the adjoint. Unfortunately, using this approach the number of forward and backward simulations is proportional to the number of optimization parameters. Hence, for the assimilation of production data this method is in most cases computationally infeasible.

In Van Essen et al. (2011), also an alternative method is introduced to solve the hierarchical optimization problem without explicitly calculating the null-space with respect to equation (7). It uses an 'on-off' type weighted objective function with weighting functions Ω_1 and Ω_2:

$$W = \Omega_1(V) \cdot V + \Omega_2(V) \cdot J \tag{8}$$

where Ω_1 and Ω_2 are 'switching' functions of V and J that take on values of 1 and 0 ('on' and 'off') or vice versa,

$$\Omega_1(V) = \begin{cases} 1 & \text{if } V - V_{\min} > \varepsilon \\ 0 & \text{if } V - V_{\min} \le \varepsilon \end{cases}, \qquad \Omega_2(V) = \begin{cases} 0 & \text{if } V - V_{\min} > \varepsilon \\ 1 & \text{if } V - V_{\min} \le \varepsilon \end{cases} \tag{9}$$

Here, ε is the threshold value as defined in inequality constraint equation (7). The gradients of W with respect to the model parameters $\boldsymbol{\theta}$ for iteration $n+1$ is then simply,

$$\left.\frac{\partial W}{\partial \boldsymbol{\theta}}\right|_{n+1} = \Omega_1(V_n) \cdot \left.\frac{\partial V}{\partial \boldsymbol{\theta}}\right|_{n+1} + \Omega_2(V_n) \cdot \left.\frac{\partial J}{\partial \boldsymbol{\theta}}\right|_{n+1} \tag{10}$$

Solving the secondary optimization problem sequentially, using W as defined in equation (8), gives improving directions for either V or J. With each iteration, the value of J either increases while the value of V decreases or the other way around, as the solution moves to and from the feasible region with respect to inequality constraint equation (7). If there exist redundant DOF with respect to the primary problem, improvement of J is possible while satisfying equation (7) and convergence of the hierarchical optimization will occur in a 'zig-zag' fashion, as schematically represented in Figure 1.

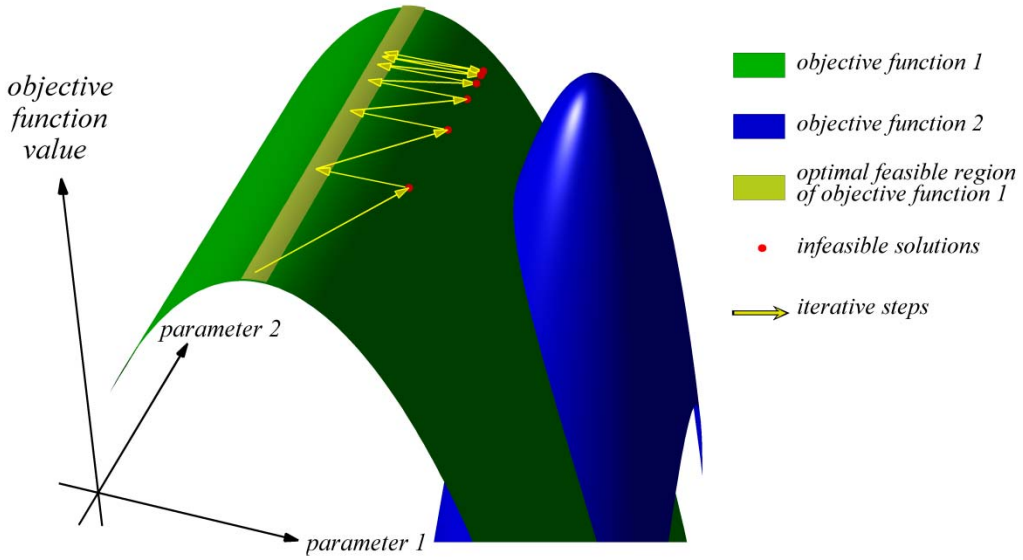

Figure 1: Schematic representation of the iterative process of solving a hierarchical optimization problem using a weighted objective function, as described by Eq. 8. The process converges towards a final solution in a 'zigzag'-fashion, moving into and out of the feasible region bounded by the optimal solutions of the primary objective function. (After Van Essen et al. 2011).

To improve convergence speed, as presented above and in Van Essen et al. (2011), a small adaptation to the switching algorithm can be made. By projecting the gradients of secondary objective function J onto the first-order approximation of the null-space of the primary objective function V, the resulting update of $\mathbf{\theta}$ will keep V closer to V_{min}. Mathematically this becomes

$$\frac{\partial \tilde{J}}{\partial \mathbf{\theta}} = \frac{\partial J}{\partial \mathbf{\theta}} \mathbf{P}_{\perp} = \frac{\partial J}{\partial \mathbf{\theta}} \left(\mathbf{I} - \mathbf{P}_{\parallel} \right) = \frac{\partial J}{\partial \mathbf{\theta}} \left(\mathbf{I} - \frac{\frac{\partial V}{\partial \mathbf{\theta}}^T \frac{\partial V}{\partial \mathbf{\theta}}}{\frac{\partial V}{\partial \mathbf{\theta}} \frac{\partial V}{\partial \mathbf{\theta}}^T} \right), \tag{11}$$

where we use the convention that the derivative of a scalar with respect to a vector is a row vector. $\mathbf{P}_{\parallel}$ is a matrix that projects $\partial J / \partial \mathbf{\theta}$ on $\partial V / \partial \mathbf{\theta}$ and $(\partial J / \partial \mathbf{\theta})\,\mathbf{P}_{\perp}$ is the orthogonally complementary projection which ensures that the step towards the secondary objective function is taken in a direction (near-)parallel to the 'ridge' in the primary objective function. Inserting equation (11) in equation (8) gives an alternative switching search direction $\mathbf{d}$ for solving the hierarchical optimization problem

$$\mathbf{d}_{n+1} = \Omega_1 \left(V_n \right) \cdot \left. \frac{\partial V}{\partial \mathbf{\theta}} \right|_{n+1} + \Omega_2 \left(V_n \right) \cdot \left. \frac{\partial J}{\partial \mathbf{\theta}} \right|_{n+1} \left(\mathbf{I} - \frac{\left. \frac{\partial V}{\partial \mathbf{\theta}} \right|_{n+1}^T \left. \frac{\partial V}{\partial \mathbf{\theta}} \right|_{n+1}}{\left. \frac{\partial V}{\partial \mathbf{\theta}} \right|_{n+1} \left. \frac{\partial V}{\partial \mathbf{\theta}} \right|_{n+1}^T} \right). \tag{12}$$

The switching algorithm using the projected gradient $\mathbf{d}$ was used in the following example to illustrate the performance of the method.

4. Primary and secondary objective functions

Two different reservoir models are used in this paper with the goal of determining lower and upper bounds on the expected economic performance over the remaining life of the field by changing the permeability field, while the model stays compliant with historic data over the history matching period. Consequently the primary objective function, $V(\mathbf{\theta})$, is defined as data mismatch between observations and simulated data:

$$V\left(\mathbf{\theta}\right) = \left(\mathbf{d} - \mathbf{h}\left(\mathbf{\theta}\right)\right)^T \mathbf{P}_v^{-1} \left(\mathbf{d} - \mathbf{h}\left(\mathbf{\theta}\right)\right), \tag{13}$$

where **θ** is a vector of unknown model parameters, **d** is a vector of data (measurements), **h** is a vector valued-function that relates the model parameters to the model outputs (i.e. the simulated data), and $\mathbf{P}_v$ is a covariance matrix of data errors.

The secondary objective function, J, is of an economic type, generally NPV,

$$J = \sum_{k=1}^{K} \left(\frac{\sum_{j=1}^{N_{prod}} \left[r_{wp} \cdot \left(y_{wp,j} \right)_k + r_o \cdot \left(y_{o,j} \right)_k \right] - \sum_{j=1}^{N_{inj}} \left[r_{wi} \cdot \left(y_{wi,j} \right)_k \right]}{(1+b)^{\frac{t_k}{\tau_t}}} \Delta t_k \right), \tag{14}$$

where $y_{wp,j}$ is the water production rate of well j, $y_{o,j}$ is the oil production rate of well j, $y_{wi,j}$ is the water injection rate of well j, r_{wi}, r_{wp} and r_o are water injection costs, water production costs and oil revenue respectively, Δt_k is the time interval of time step k in days, b is the discount rate for a reference time τ_t, and N_{inj} and N_{prod} are the number of injection and production wells.

5. Egg model example

In this first example, initially presented by Van Essen et al. (2010), we consider a three-dimensional oil reservoir model, introduced for a different purpose in van Essen et al. (2009). The reservoir model consists of 18,553 active grid blocks, as depicted in Figure 2, and has dimensions of 480×480×28 m. Its geological structure involves a network of fossilized meandering channels of high permeability. The average reservoir pressure is 40.0 MPa. All remaining geological and fluid properties used in this example are presented in Table 1. The reservoir model contains eight injection wells and four production wells. The near-wellbore flow is modeled using a Peaceman well model.

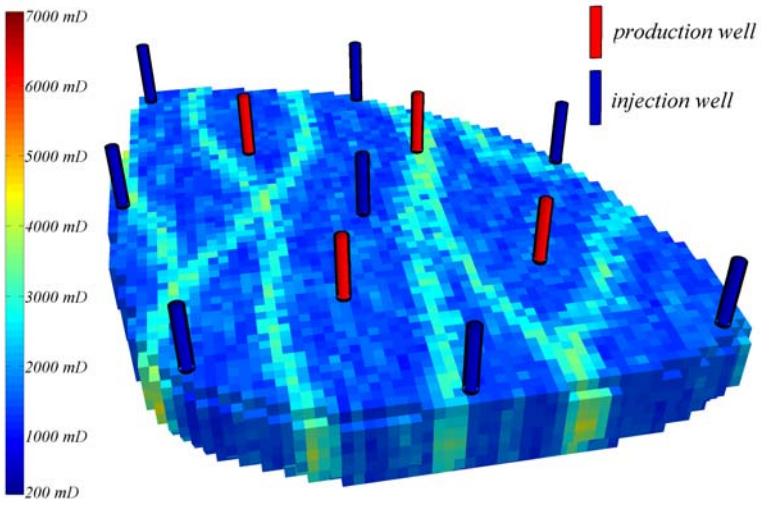

Figure 2: Three-dimensional oil reservoir model with eight injection and four production wells, after Van Essen et al., 2009. Its geological structure involves a network of fossilized meandering channels of high permeability in a low-permeability background.

Table 1: Geological and fluid properties for the example			
Symbol	*Variable*	*Value*	*Units*
φ	Porosity	0.20	-
ρ_o	Oil density	800	kg/m^3
ρ_w	Water density	1000	kg/m^3
c_o	Oil compressibility	1.00×10^{-10}	1/Pa
c_w	Water compressibility	1.00×10^{-10}	1/Pa
μ_o	Dynamic oil viscosity	5.00×10^{-3}	Pa s
μ_w	Dynamic water viscosity	1.00×10^{-3}	Pa s
p_c	Capillary pressure	0	Pa

During the first 1.5 years of production from the reservoir, the bottomhole pressures of the producers are kept at a constant value of 39.5 MPa. During that time, the injection rates of all eight injectors are prescribed to fluctuate monthly with a uniform probability distribution around an average value of 5.52×10^{-4} m^3/s (300 bbl/day) and a maximal offset ± 9.2×10^{-4} m^3/s (50 bbl/day). Monthly production measurements are taken of the flowing bottomhole pressures of the eight injectors and the oil and water rates of the four producers, on top of which no noise is superimposed. Thus, the total number of measurements is 288.

In this example historic data are available over the first 1.5 years of production and lower and upper bounds on expected economic performance are determined over the remaining life of the field – from 1.5 to 6.0 years – by changing model properties (gridblock permeabilities) , while the model stays compliant with historic data over the first 1.5 years of production. In this example the water injection costs r_{wi}, the water production costs r_{wp} and the oil revenue r_o are assumed constant at values of 0 \$/m^3, -1 \$/m^3 and 9 \$/m^3 respectively. The discount rate, b, in this example is zero. The upper and lower bounds of the NPV can only be determined for a given (fixed) control strategy. In this example, a reactive control approach is used that is evaluated on a field level. All injection wells are assumed to continuously operate on their average injection rate of 5.52×10^{-4} m^3/s and the production wells on their fixed bottomhole pressure of 39.5 MPa. The instant that the field watercut exceeds 0.90, all wells are shut-in. Note that this threshold is related to the ratio between oil revenue r_o and water production costs r_{wp}. To determine the history-matched models that provide the lower and upper bound on NPV for the remaining producing life, two hierarchical optimization procedures are initiated. They terminate when the feasible updates no longer result in a significant change in NPV. Figure 3 depicts the measured production data, along with the simulated production data originating from the final lower and upper bound model, resulting from the hierarchical optimization method. It shows that the errors between measured and simulated bottomhole pressures of the injectors and fractional flow rates of the producers are very small for both the lower and upper bound models. Thus, the condition that the updated models maintain a good history match is met. However, in Figure 4 it can be observed that the permeability fields of both models are quite different. These differences have a large impact on the predicted production data given the assumed reactive production strategy, as can be observed in Figure 5. Moreover the change in permeability in the near-well areas around the injectors has a strong effect on the pressure response of the injectors. Finally, Figure 6 shows the actual lower and upper bounds on predicted NPV over time, in terms of NPV for the entire producing reservoir life (6 years), and in terms of incremental NPV for just the remaining (future) producing reservoir life (4.5 years). It can be observed that the upper and lower bounds of the incremental NPV are 63% above and below their average value.

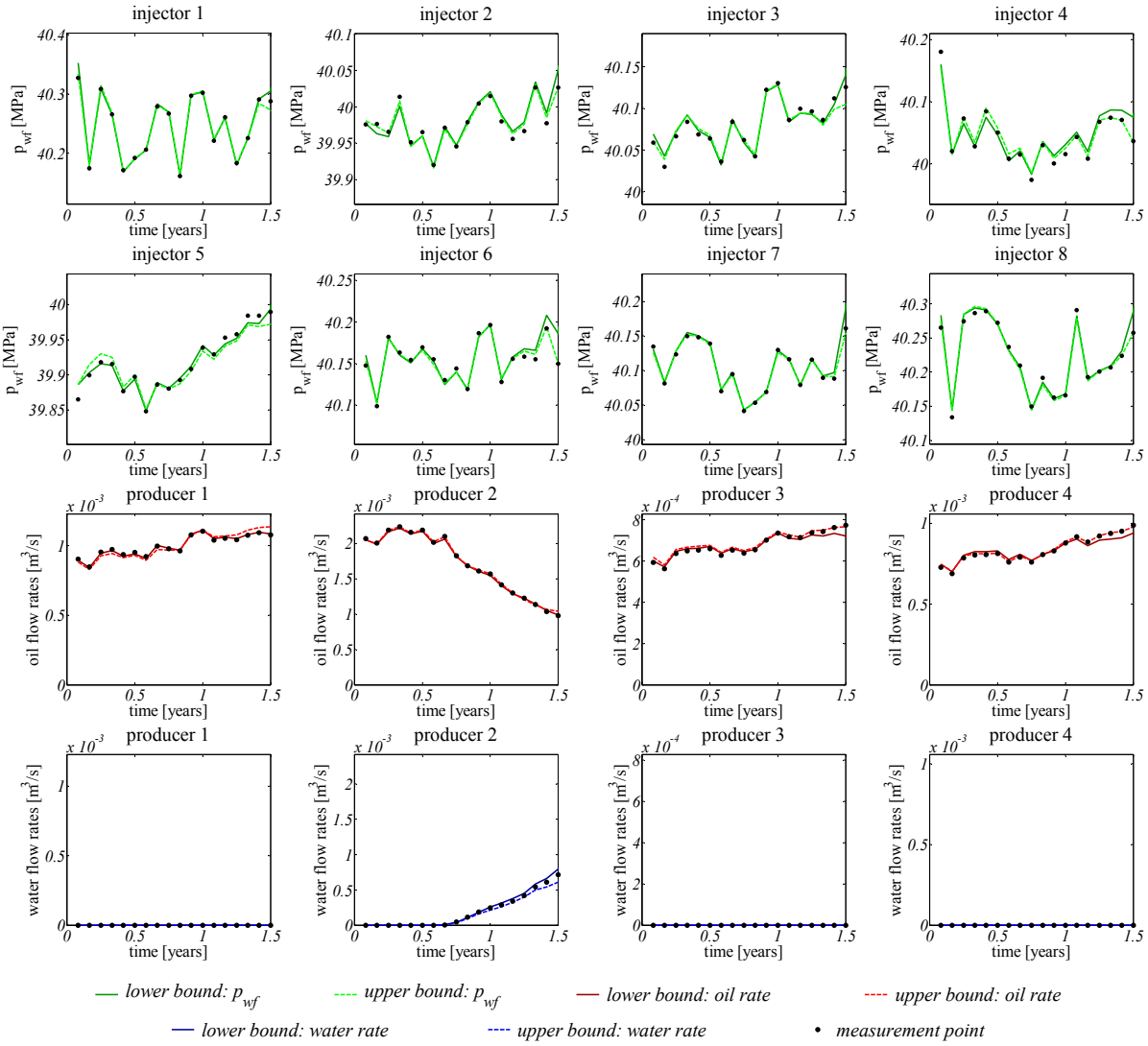

Figure 3: Measured production data of the first 1.5 years of production from the (synthetic) 3D reservoir, along with the simulated production data originating from the lower and upper bound models.

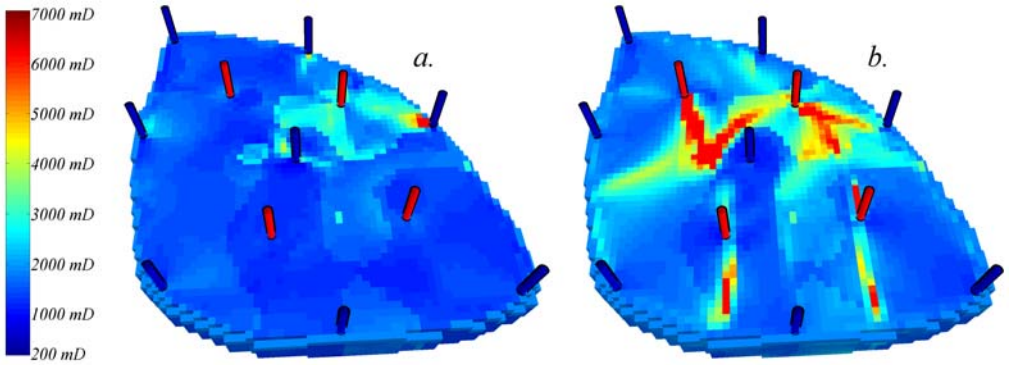

Figure 4: Permeability fields of the lower bound 3D reservoir model (a) and upper bound 3D reservoir model (b) determined after the first 1.5 years of production.

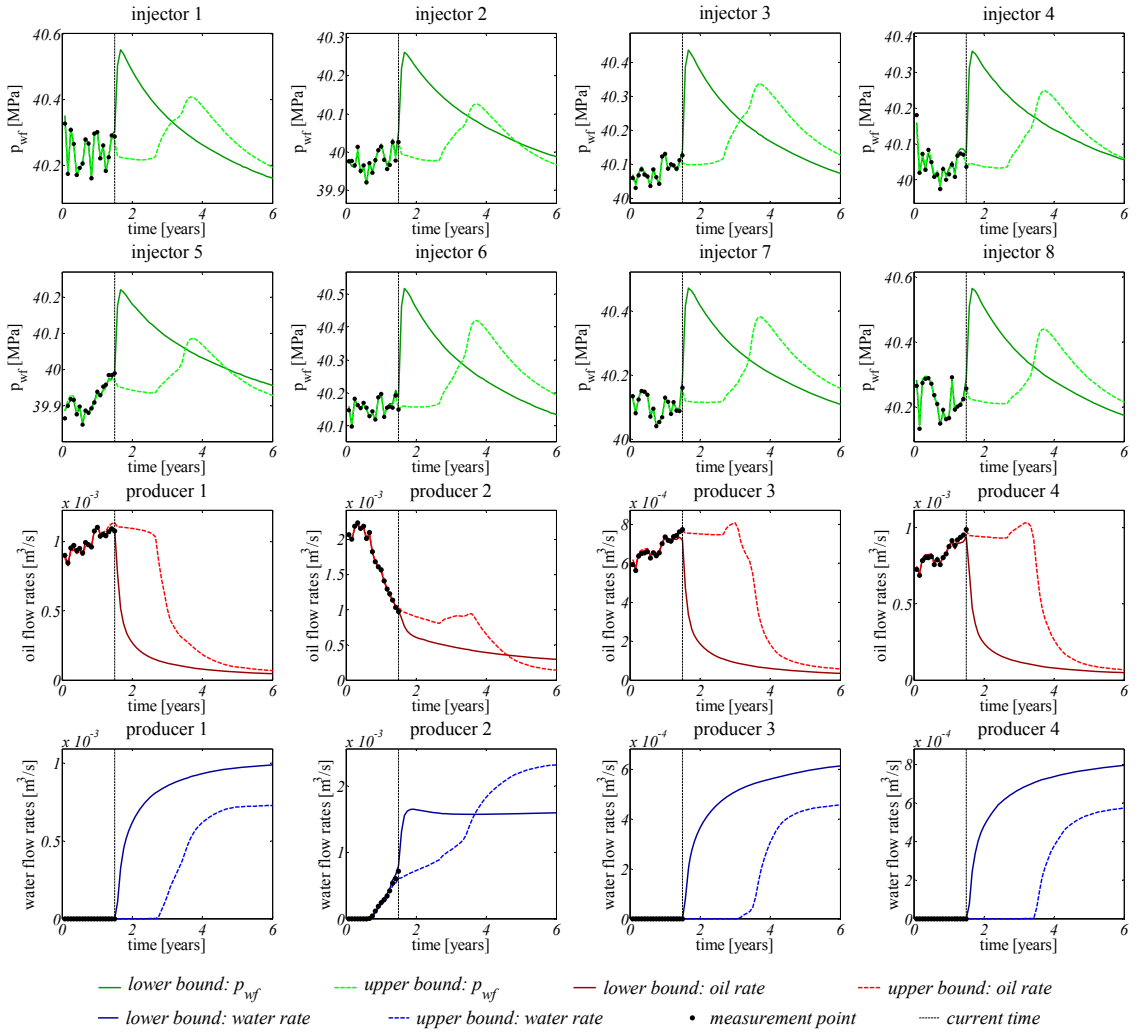

Figure 5: Measured production data of first 1.5 years of production from the (synthetic) 3D reservoir, along with the simulated production data for the remaining 4.5 years of production until the end of the field's life, originating from the lower and upper bound models.

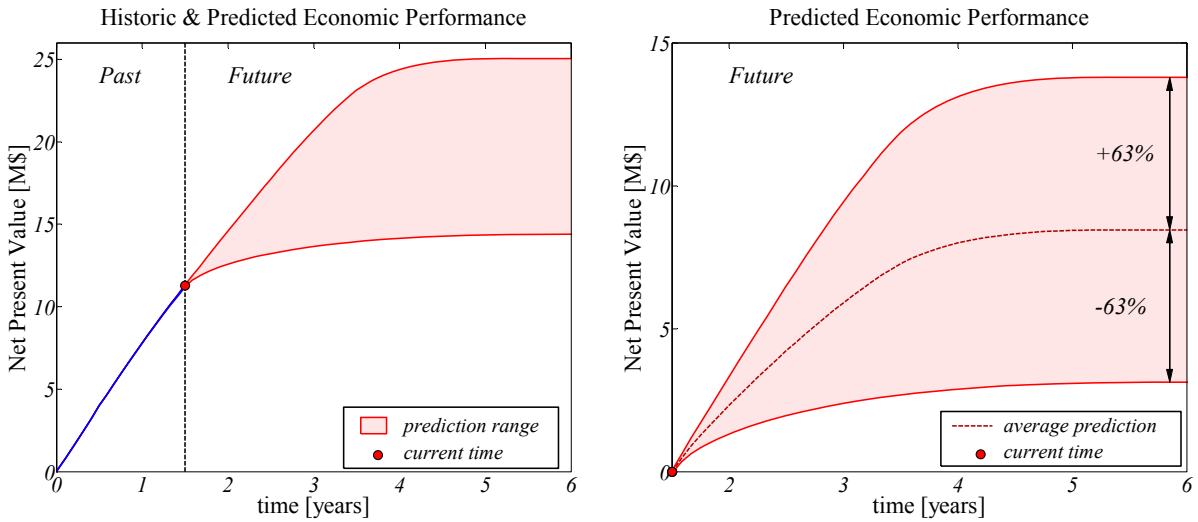

Figure 6: NPV over time for the lower and upper bound reservoir models. The plot on the left shows both the historic (first 1.5 year) and future (from 1.5 to 6 years) increase in NPV over time. The plot on the right side only shows the incremental NPV for the remaining (future) 4.5 years of production.

6. Brugge model example

In the second experiment we use data from the Brugge benchmark workshop organized in 2009 (Peters et al., 2010, 2013). In the original bench mark study, the 'truth' case used to generate the data was not disclosed and therefore, in this work we use a new 'truth' honouring all well logs, geological descriptions distributions of geological model parameters, porosity/permeability relations and the geological structure of the Brugge field. Figure 7 depicts the new 'true' Brugge permeability field, which is used to generate synthetic data. Blue and red bars in Figure 7 represent injectors and producers respectively. The fluid properties and Corey exponents used in this example are given in Table 2.

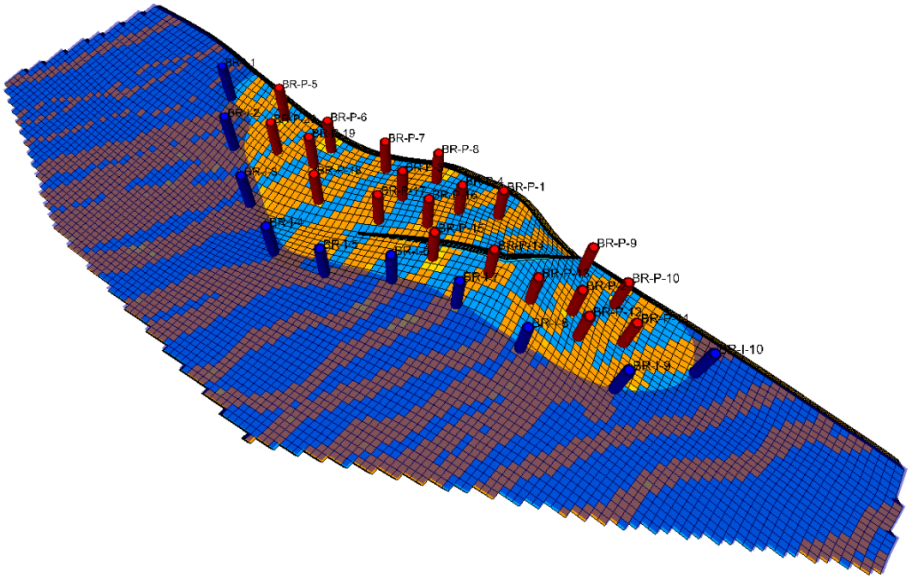

Figure 7: Permeability field with 11 injection wells and 20 production wells. The blue surface indicates the oil-water contact.

Table 2: Fluid properties and Corey exponents for the Brugge field example.

Symbol	Variable	Value	Units
ρ_o	Oil density	897	kg/m^3
ρ_w	Water density	1000.28	kg/m^3
c_o	Oil compressibility	10.3×10^{-10}	1/Pa
c_w	Water compressibility	4.35×10^{-10}	1/Pa
μ_o	Dynamic oil viscosity	1.29×10^{-3}	Pa s
μ_w	Dynamic water viscosity	0.32×10^{-3}	Pa s
S_{wc}	Connate water saturation	0.266	-
S_{or}	Residual oil saturation	0.15	-
k^0_{rw}	End point water rel perm	0.6	-
k^0_{ro}	End point oil rel perm	0.4	-
n_w	Water Corey exponent	3	-
n_o	Oil Corey exponent	5	-

The reservoir model consists of 60,048 active grid blocks, and has dimensions of 3km×10km×80 m. It contains 11 injection wells located near the rim of the oil-water contact at a depth of 1678m from the surface and 20 production wells, as depicted in Figure 7. Wells are located in the grid block centers, and we use a standard Peaceman well inflow model. During the first 10 years of production (the history matching period) all production wells are constrained to a minimum pressure of 4.9 MPa and a maximum liquid rate of 3.7×10^{-3} m^3/s and all injection wells operate at a constant water flow rate of 7.4×10^3 m^3/s. Moreover, production wells are shut-in individually if the water fraction in the produced liquid is above 90%. After the history matching period (10

years), closed wells are reopened. Wells are drilled according to the time scheme presented in the Brugge workshop (Peters, et al., 2009).

6.1. Historical data

In this example historical data are available over the first 10 years of production and lower and upper bounds on expected economic performance are determined over the remaining life of the field – from 10 to 30 years – by changing the permeability field, while the model stays compliant with historic data over the first 10 years of production. Time-lapse seismic data as well as production data are used as historic data. Production data consist of periodic measurements of water and oil rates in the producers. Independent measurement errors are generated from Gaussian distributions with zero mean and standard deviations equal to 10% percent of the original measurements. Negative production rates, after the addition of noise, are reset to zero. Because the measurement errors are independent, the error covariance matrix is diagonal.

6.2. Multi-objective optimization settings

Using equation (13) as the primary objective function and equation (14) as the secondary objective function two hierarchical optimization procedures are conducted to determine the history-matched models that provide the lower and upper bounds on NPV for the remaining producing life. The procedures are terminated when the feasible updates no longer result in a significant changes in objective function value. The starting point for the assisted history matching process (primary objective function) is selected randomly out of 104 available prior models in the Brugge data set. The prior model is iteratively conditioned to historical data by adjusting the horizontal gridblock permeability values. In this experiment the water injection cost r_{wi}, the water production cost r_{wp} and the oil revenue r_o are assumed constant at values of 5 \$/bbl, -5 \$/bbl and 80 \$/bbl respectively. The discount rate, b, is set to 10%.

6.3. Results: History matching based on production data

In this example, history matching is performed based on production data. We constrain the search space of the secondary problem by choosing the threshold value of equation (7) as 0.5% of the minimum of the primary objective function. Figure 8 depicts the historical data and the lower and upper bounds of water production in the first eight producers as an example of the typical ranges of the bounds. The history matching and forecasting periods are separated by a dashed line. Blue and red colours represent the lower and upper bounds of oil and water production. Figure 9 despicts the the injection pressures in the firs four injectors. Unlike in the results for the previous example, depicted in Figure 5, there is no jump in the pressures at the beginning of the forecasting period because they have already reached their maximum allowable values. Figure 10 depicts the historical data and the lower and upper bounds for the cumulative oil and water production of the entire field.

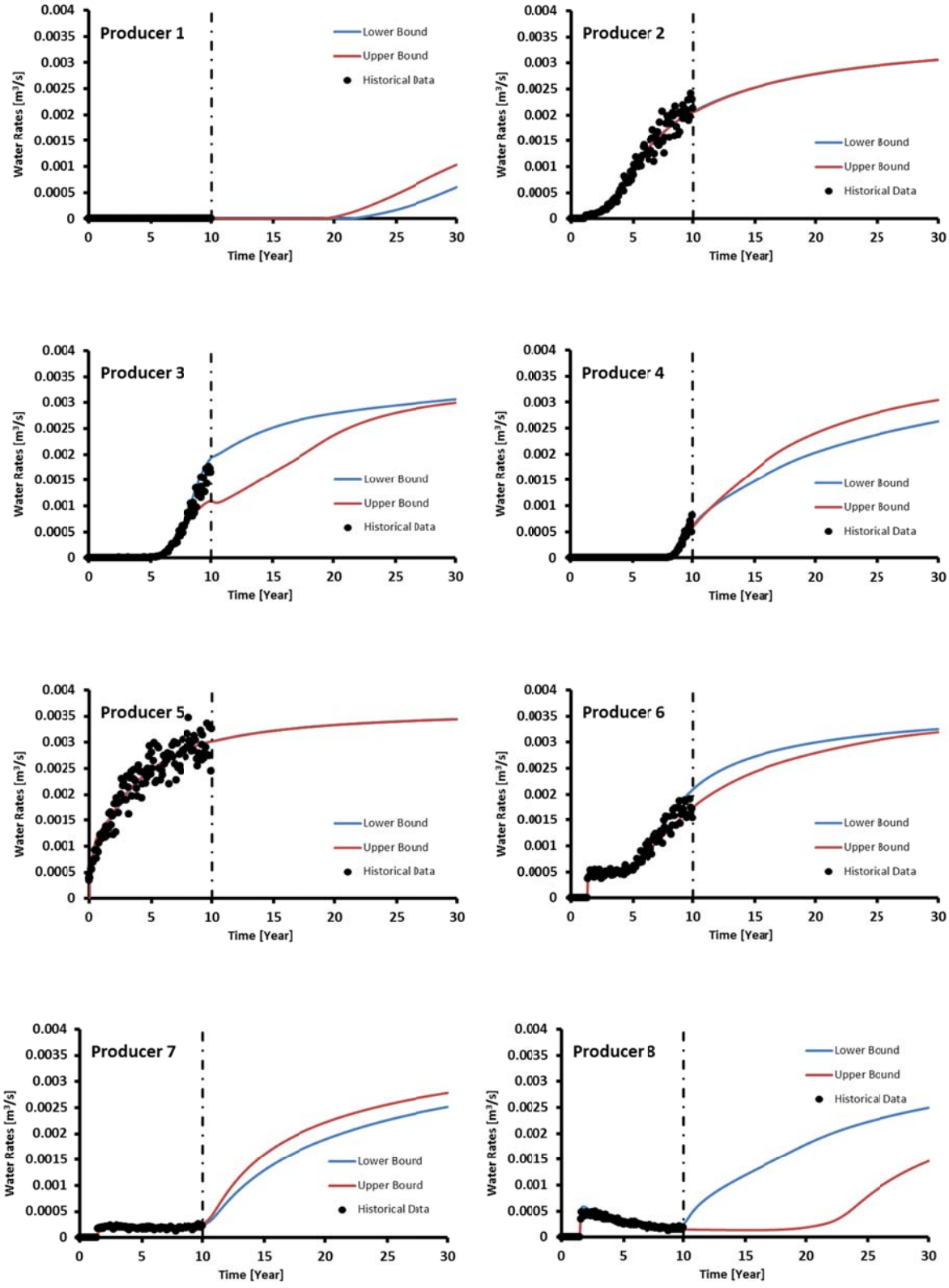

Figure 8: Historical and predicted water production over 30 years of production for the first eight producers for the Brugge field example.

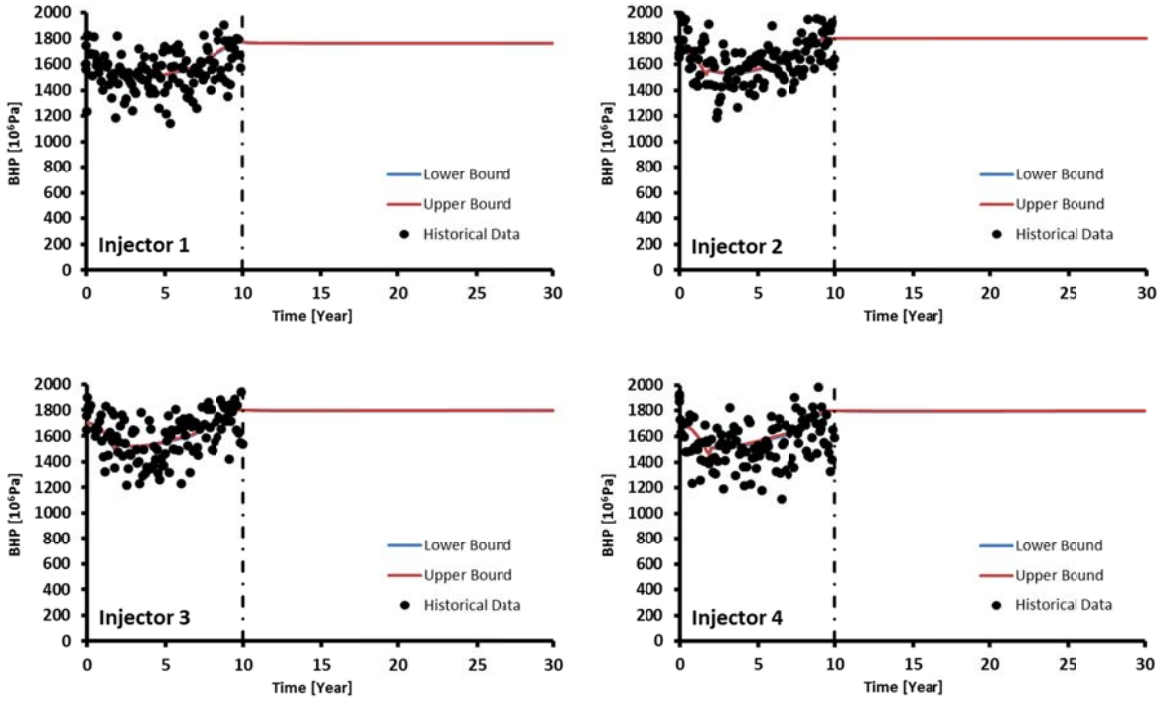

Figure 9: Historical and predicted injection pressures over 30 years of production for the first four injectors for the Brugge field example.

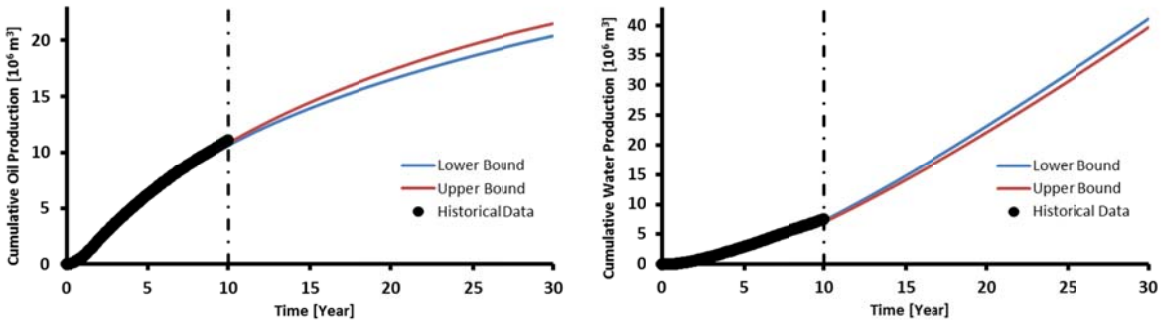

Figure 10: Historical and predicted cumulative oil production (left) and water production (right) over 30 years of production.

As can be seen in Figure 10 the lower bound and upper bound models produce the same history but different forecast. Moreover Figure 11 depicts the economic performance (NPV) of the upper and lower bound models over time for the entire production life, including the history and the prediction. In this experiment the incremental NPV of the upper bound model is 19.5% higher than the incremental NPV of the lower bound model.

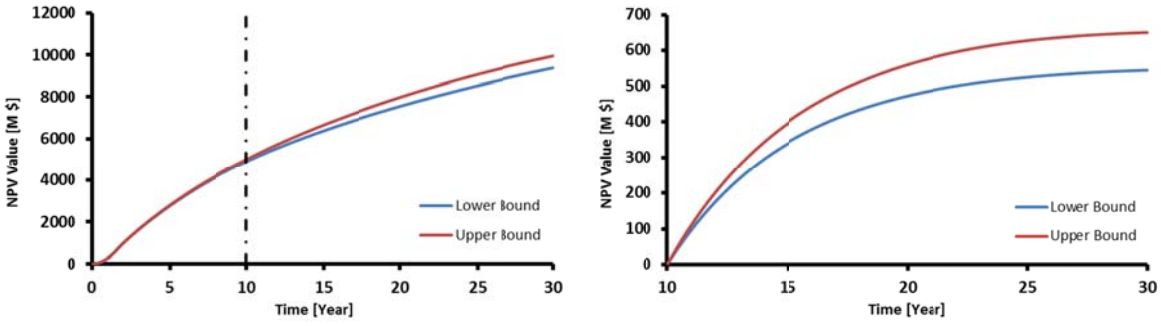

Figure 11: NPV over time for the lower and upper bound reservoir models. The plot on the left shows both the

historic (first 10 years) and future (from 10 to 30 years) increase in NPV over time. The plot on the right side only shows the incremental NPV for the remaining (future) 20 years of production. Note that the right figure is a blown-up version of a part of the left one.

Figure 12 shows the differences between the lower and upper bound permeability fields for all nine layers of the field. It can be observed in Figure 12 that the permeability fields of both models are different, especially in the producing layers. These differences have an impact on the predicted production data while they result in the same production history, as can be observed in Figure 10. We note that although the permeability values away from the wells are more likely to be in the null space (i.e. to have room for variation), they also have less of an effect on the output in the wells. Apparently the optimization algorithm did not produce significant changes in these values because that would not have changed the resulting NPV. Computation of these result required 200 pairs of forward and backward (adjoint) simulations, where each pair took, on average, 786 s.

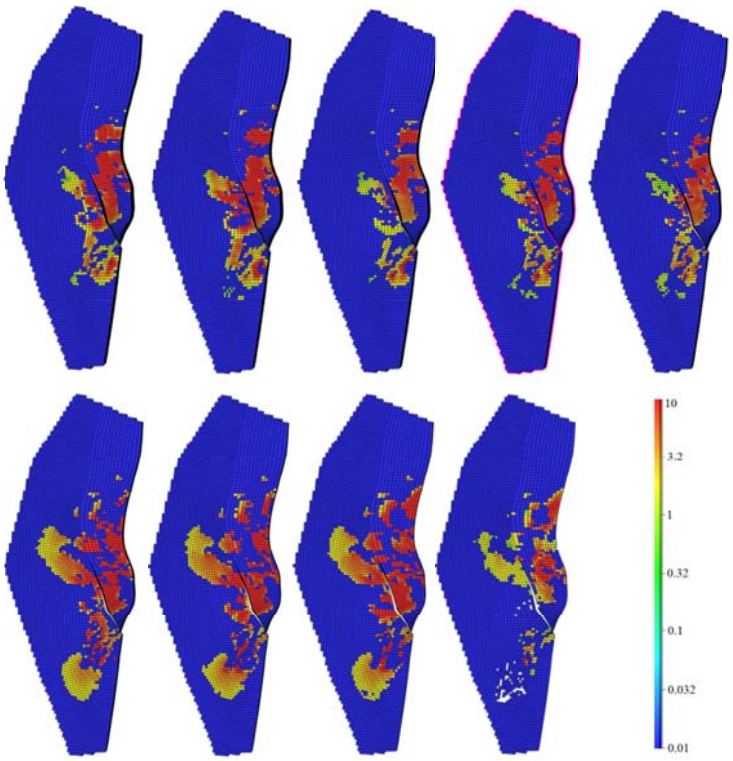

Figure 12: Difference between the lower and upper bound permeability fields. All permeability values are expressed as the natural logarithm of permeability in mD.

6.4. Effect of data type

In the previous section we obtained the lower and upper bound models based on production data. In order to investigate the effect of data type on the upper and lower bound models, two more experiments are conducted based on different data types. In the first experiment the upper and lower bound models are obtained based on interpreted time lapse seismic data (saturation maps) and production data. The saturation maps are generated by simulating the "truth" and adding independent measurement errors by sampling from a Gaussian distribution with zero mean and standard deviations equal to 10% percent of the simulated saturation values. As before, we constrain the search space of the secondary problem by choosing the threshold value of equation (7) as 0.5% of the minimum of the primary objective function. The second experiment involves assimilation of both time-lapse seismic and production data while also prior information is added to the primary objective function as a regularization term. Figure 13 shows the incremental NPV difference between the lower and upper bound models obtained using different data types. As can be seen in Figure 13, the incremental NPV difference decreases by adding more information.

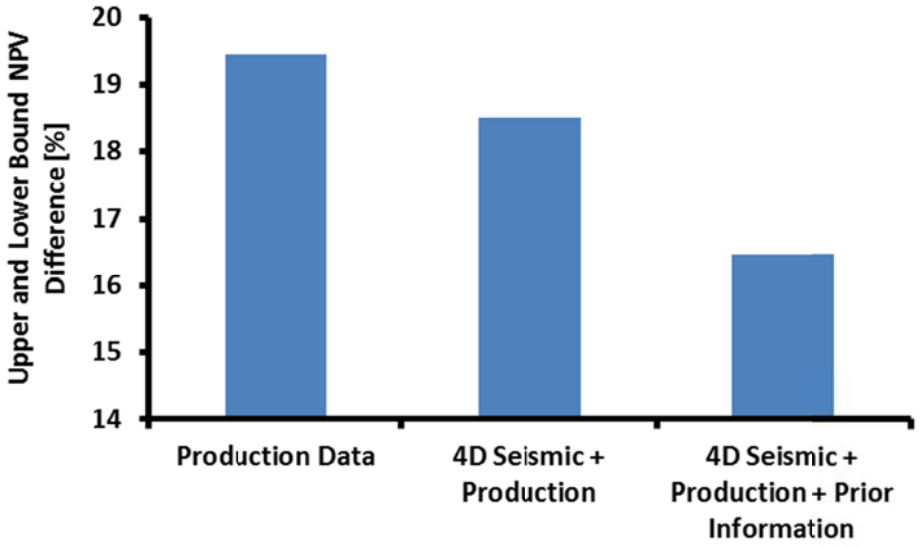

Figure 13: Difference between the upper bound and lower bound incremental NPV values for models obtained based on different data types.

6.5. Effect of threshold value

In this section we investigate the effect of the threshold value, ε, in equation (7). We constrain the search space of the secondary problem to different extents by choosing a range of threshold values varying between 0.15% and 1.5% of the minimum of the primary objective function. Interpreted time-lapse seismic data (saturation maps) and production data formed the historical data, and two hierarchical multi-objective optimizations were conducted to find the lower and bounds for the reservoir model for different threshold values. Figure 14 shows the incremental NPV difference between the upper and the lower bound models versus the threshold value ε.

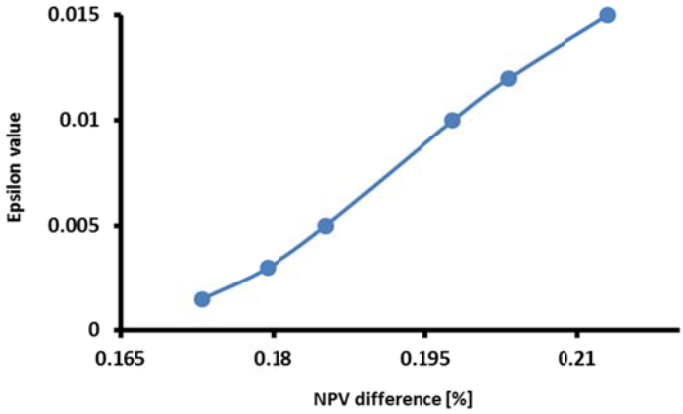

Figure 14: Incremental NPV difference between the upper bound and the lower bound model for different epsilon values.

Figure 15 depicts how the primary and secondary objective functions change for different values of ε. Figure 14 and Figure 15 show that as the threshold value in equation (7) increases the difference between the lower and upper model values of incremental NPV increases also. However, the effect is not very large and even for the lowest threshold value ($\varepsilon = 0.15\%$), a difference of approximately 17% in incremental NPV is obtained.

We note that the lower and upper bounds have been obtained by a gradient-based optimization technique which may have resulted in local rather than global optima. Lower lower bounds and higher upper bounds may therefore exist.

We also note that both the red and the blue curves can be interpreted as parts of (approximate) Pareto curves. Points on a Pareto curve are at the boundary of the feasible set of solutions in the bi-objective space, and recently several studies have been performed to characterise a full Pareto curves for bi-objective flooding optimization;

see, e.g., Liu and Reynolds (2016). Such a curve gives the decision maker the opportunity to select between competing objectives, i.e. to achieve a large value of the secondary objective function at the price of a strong drop in the primary objective function value, or a somewhat smaller secondary objective function value without losing much of the primary objective function value.

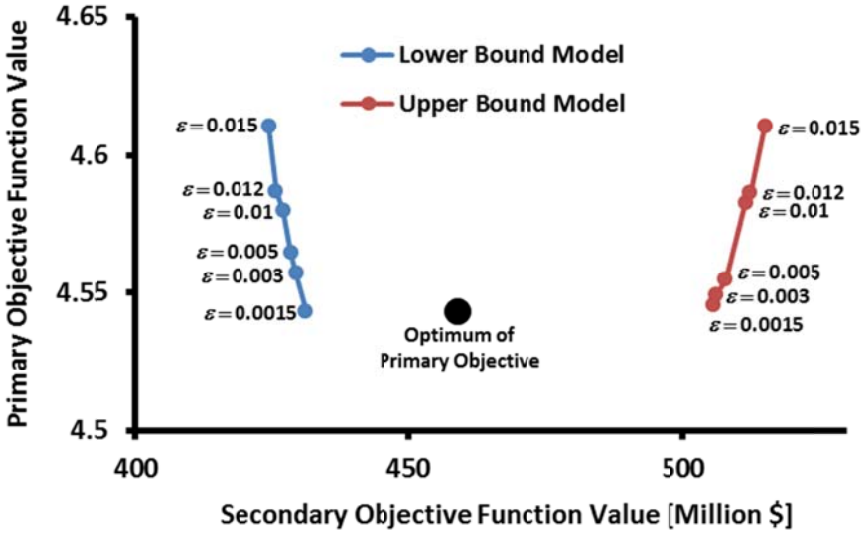

Figure 15: Secondary objective function value versus its corresponding primary objective function value, both expressed as incremental NPV.

7. Discussion

In the current paper we used gridblock permeabilities as history matching parameters. However the proposed method could equally well be applied using other parameters, e.g. porosities, fault multipliers or aquifer strength. Moreover, other data types than the production data and interpreted time-lapse seismic that we used could be assimilated. We note that the use of gradients with respect to the history matching parameters is an important ingredient in our method. This implies that we need a technique to compute those gradients. We used an adjoint method, which is computationally very efficient. However it is, in theory, also possible to implement our method using approximate gradients obtained with e.g. the simultaneous perturbation stochastic approximation (SPSA) technique, see Spall (1998), or ensemble optimization (EnOpt); see Chen et al. (2009) for the basics of the method and Fonseca et al. (2014) for an implementation in hierarchical optimization. The latter (EnOpt) approach also allows for the inclusion of uncertainty in the reservoir models; see Fonseca et al. (2015).

We note that our method has theoretical links to the use of level sets to relax the primary objective function constraint in hierarchical optimization as discussed in the last paragraph of Section 2. Moreover, we note that other weak-constrained optimization methods could be applied to solve the hierarchical optimization problem. The current implementation has shown to be robust in various applications using both adjoint-based and ensemble-based techniques (Van Essen et al. (2011), Chen et al. (2012), Fonseca et al. (2014).

The determination of lower and upper bounds of future production using different types of data, as performed in the Brugge example, can be interpreted as a means to assess the cost effectiveness of acquiring different data types to reduce the uncertainty in the expected NPV. It is tempting to interpret this as a way to assess the value of information (VOI) of those measurements but because we do not know the statistical properties of the forecasted NPV we can not draw conclusions about the change in expected value of those forecasts and therefore our method does not truly provide the VOI. (For detailed information about the the concept of VOI see Bratvold et al., 2009 or Eidsvik et al., 2015.)

8. Conclusions

In this paper, we presented a hierarchical optimization method to determine lower and upper bounds on predicted production from history-matched models. We conclude that:

- The non-uniqueness of history matched models implies that future production can only be predicted within bounds.

- The non-uniqueness implies the presence of remaining degrees of freedom after history matching (i.e. after solving the primary optimization problem) which can be used to determine lower and upper bounds on future production through solving two secondary optimization problems.
- The method proposed in our paper provides a way to gain more insight in the possible economic consequences of the lack of information in historic data. These consequences can be represented by total production, ultimate recovery, (incremental) NPV or any other economic measure.
- The method is not limited to historic production data. Alternative data sources, e.g. time-lapse seismic data, can be used to determine the impact on the predicted economic performance. Hence, this method may also play a role in the quantification of the value of information.
- Introducing more data sources, e.g. time-lapse seismic or prior information, results in smaller differences in economic performance (incremental NPV) between the lower and upper bound models.

9. Acknowledgements

This research was carried out within the context of the Recovery Factory programme, a joint project of Shell Global Solutions International and Delft University of Technology. We thank Shell for making available to us their in-house reservoir simulator DynamoMores.

10. References

Aanonsen, S. I., Nævdal, G., Oliver, D. S., Reynolds, A. C. and Vallès, B. 2009. The Ensemble Kalman Filter in Reservoir Engineering--a Review. *SPE Journal* 14 (3) 393-412. DOI: 10.2118/117274-PA

Bratvold, R. B., Bickel, J. E., & Lohne, H. P. 2009. Value of information in the oil and gas industry: past, present, and future. *SPE Journal* **12** (4) 630-638. DOI: 10.2118/110378-PA

Chen, Y., Oliver, D.S. and Zhang, D. 2009. Efficient ensemble-based closed-loop production optimization. *SPE Journal* **14** (4) 634-645. DOI: 10.2118/112873-PA

Chen, C., Li, G., Reynolds, A., et al., 2012. Robust constrained optimization of short-and long-term net present value for closed-loop reservoir management. *SPE Journal* **17** (03) 849–864, DOI: 10.2118/141314–PA

den Dekker, A.J., Bombois, X. and Van den Hof, P.M.J. 2008. Finite sample confidence regions for parameters in prediction error identification using output error models. Proc. 17th IFAC World Congress, Seoul, Korea, 6-11-July, pp. 5024-5029.

Eidsvik, J., Mukerji, T. and Bhattacharjya, D., 2015: *Value of information in the earth sciences.* Cambridge University Press, Cambridge.

Evensen, G. 2009. *Data assimilation: the ensemble Kalman filter*. Springer, Berlin.

Fonseca, R.M., Leeuwenburgh, O., Van den Hof, P.M.J. and Jansen, J.D. 2014. Ensemble-based hierarchical multi-objective production optimization of smart wells. *Computational Geosciences*. **18** (3-4) 449–461. DOI: 10.1007/s10596-013-9399-2

Fonseca, R.M., Leeuwenburgh, O., Della Rossa, E., Van den Hof, P.M.J. and Jansen, J.D., 2015: Ensemble-based multi-objective optimization of on-off control devices under geological uncertainty. *SPE Reservoir Evaluation and Engineering* **18** (4) 1094-6470. DOI: 10.2118/173268-PA

Haimes, Y. Y. and Li, D. 1988. Hierarchical multiobjective analysis for large-scale systems: Review and current status. *Automatica* **24** (1) 53-69. DOI: 10.1016/0005-1098(88)90007-6

Jansen, J.D. 2011. Adjoint-based optimization of multiphase flow through porous media – a review. *Computers and Fluids* **46** (1) 40-51. DOI: 10.1016/j.compfluid.2010.09.039

Kraaijevanger, J. F. B. M., Egberts, P. J. P., Valstar, J. R. and Buurman, H. W. 2007. Optimal waterflood design using the adjoint method. Paper 105764 presented at the SPE Reservoir Simulation Symposium, Houston, Texas, U.S.A., February. DOI: 10.2118/105764-MS

Liu, X. and Reynolds, A.C. 2016. Gradient-based multiobjective optimization with applications to waterflooding optimization. *Computational Geosciences* **20** (3) 677–693. DOI: 10.1007/s10596-015-9523-6

Marler, R. T. and Arora, J. S. 2004. Survey of multi-objective optimization methods for engineering. *Structural and multidisciplinary optimization* **26** (6) 369-395. DOI: 10.1007/s00158-003-0368-6

Oliver, D.S., Reynolds, A.C. and Liu, N. 2008. *Inverse theory for petroleum reservoir characterization and history matching*, Cambridge University Press, Cambridge.

Peters, E., Chen, Y., Leeuwenburgh, O. and Oliver, D. S. 2013. Extended Brugge benchmark case for history matching and water flooding optimization. *Computers & Geosciences* **50** 16-24. DOI: 10.1016/j.cageo.2012.07.018

Peters, L., Arts, R., Brouwer, G., Geel, C., Cullick, S., Lorentzen, R. J., Chen, Y., Dunlop, N., Vossepoel, F. C. and Xu, R. 2010. Results of the Brugge benchmark study for flooding optimization and history matching. *SPE Reservoir Evaluation & Engineering* **13** (3) 391-405. DOI: 10.2118/119094-PA

Quinn, S.L., Harris, T.J. and Bacon, D.W. 2005. Accounting for uncertainty in control-relevant statistics. *Journal of Process Control*, **15** (6) 675-690. DOI: 10.1016/j.jprocont.2005.01.002.

Spall, J.C., 1998. Implementation of the simultaneous perturbation algorithm for stochastic optimization. *IEEE Transactions on Aerospace and Electronic Systems* **34** (3) 817-823. DOI 10.1109/7.705889

Tavassoli, Z., Carter, J. N. and King, P. R. 2004. Errors in History Matching. *SPE Journal* **9** (3) 352-361. DOI: 10.2118/86883-pa

Van Essen, G. M., Zandvliet, M. J., Van den Hof, P. M. J., Bosgra, O. H. and J.D., J. 2009. Robust Waterflooding Optimization of Multiple Geological Scenarios. *SPE Journal* **14** (1) 202-210. DOI: 10.2118/102913-PA

Van Essen G.M., Jansen, J.D. and Van den Hof, P.M.J. 2010. Determination of lower and upper bounds of predicted production from history-matched models. Proc. 12th European Conference on Mathematics in Oil Recovery (ECMOR XII), Oxford, UK, 6-9 September.

Van Essen, G. M., Van den Hof, P. M. J. and J.D., J. 2011. Hierarchical long-term and short-term production optimization. *SPE Journal* **16** (1) 191-199. DOI: 10.2118/124332-PA

Watson, A. T., Gavalas, G. R. and Seinfeld, J. H. 1984. Identifiability of estimates of two-phase reservoir properties in history matching. *SPE Journal* **24** (6) 697-706. DOI: 10.2118/12579-PA